GEOLOGICAL SURVEY OF CANADA
OPEN FILE 7323

Magnetotelluric Soundings from the Central Rae Domain of the Churchill Province, Nunavut.

J.E. Spratt, B. Roberts, D. Kiyan, and A.G. Jones

2013

Natural Resources Canada | Ressources naturelles Canada

Canada

GEOLOGICAL SURVEY OF CANADA
OPEN FILE 7323

Magnetotelluric Soundings from the Central Rae Domain of the Churchill Province, Nunavut.

J.E. Spratt[1], B. Roberts[2], D. Kiyan[3], and A.G. Jones[3]

[1] Magnetotelluric Consultant, Wakefield, Quebec J0X 3G0
[2] Geological Survey of Canada, 615 Booth Street, Ottawa, Ontario K1A 0E9
[3] Dublin Institute of Advanced Studies, Ireland

2013

doi:10.4095/292237

This publication is available for free download through GEOSCAN (http://geoscan.ess.nrcan.gc.ca).

Recommended citation

Spratt, J.E., Roberts, B., Kiyan, D., and Jones, A.G., 2013. Magnetotelluric Soundings from the Central Rae Domain of the Churchill Province, Nunavut; Geological Survey of Canada, Open File 7323, 34 p. doi:10.4095/292237

Publications in this series have not been edited; they are released as submitted by the author.

Table of Contents

Introduction

As part of Natural Resources Canada's GEM (Geo-mapping for Energy and Minerals) program, the Diamonds project is designed to study the deep lithosphere beneath the Slave and Churchill provinces of northern Canada. As these areas are known to host diamond-bearing kimberlites, the primary goal of this project is to develop an understanding of the potential for diamonds and reduce risk in their exploration. During the past three summer field seasons (2010, 2011, and 2012), magnetotelluric (MT) data have been acquired and analyzed throughout mainland Nunavut in order to contribute to achieving this goal. These data will enhance and complement interpretations of previous MT data collected throughout eastern Nunavut (Figure 1), with the long term goal of generating a regional 3-dimensional model of the conductivity structure of the lithosphere. In 2010 MT data were collected along a 300 km-long transect, profile 3, that extends from southwest of Repulse Bay to the south end of the Boothia Peninsula, through a portion of the Rae craton in the Churchill Province of the eastern Canadian Shield (Figure 2; Spratt et al, 2011). During the summer of 2011 MT data were collected along the northern and northwestern half of two profiles (profiles 1 and 2) extending north and northwest of Wager Bay, as well as at several isolated locations throughout the region designed to fill gaps in future 3-D models (Figure 2; Spratt et al. 2012). The summer of 2012 saw the acquisition of new data that continue along profile 1 southeastward towards the coast, south of Wager Bay, and along profile 2 to just south of Chesterfield Inlet (Figure 2). This report describes the data processing, and analysis of the 2012 MT data, as well as preliminary 2-D modelling and interpretation of the 2011 and 2012 MT data along profiles 1 and 2.

Data Acquisition and processing

The field campaign took place during the month of July and was based out of the community of Chesterfield Inlet. Broadband (BBMT) data were acquired at a total of 16 site locations, with 1 long period (LMT) site located off profile (site DMN222) for quality control and 3-D interpretations. The data have been divided into 2 separate profiles, profiles 1 and 2, for analysis and 2-D modelling (Figure 2). Incorporating data collected in 2011 and 2012, profile 1 is a 360 km-long, northwest-to-southeast profile located in the Rae Domain of the Churchill Province that consists of 18 BBMT and 3 LMT sites

that extends from the Committee Bay Block to the northwest, across the Committee Bay greenstone belt, into the Archean granitoid gneiss of the Rae domaine, and across the Wager Bay shear zone (Henderson and Broom, 1990). Profile 2 is 425 km-long, approximately north-south profile that is made up of 15 BBMT and 3 LMT sites and extends from the Committee Bay block of the Rae Domain to the north, across the Wager Bay shear zone (WBSZ), and crosses the northernmost extent of the Snowbird Tectonic Zone (STZ) that separates the Rae domaine from the Hearne domaine to the south (Hoffman, 1988).

Long period (LMT) data were collected at a single site location using the NiMS recording instrumentation. Data acquisition duration and location for this site is shown in Table 1. The electric fields were recorded in two horizontal, perpendicular directions using lead-lead-chloride porous pot electrodes and the magnetic fields were recorded in the horizontal, plus the vertical direction using a 3-component fluxgate magnetometer. The data were converted from the recorded binary format to ascii format using John Bookers conversion code and were then processed using the robust, cascade decimation code of Jones (Jones and Jödicke, 1984). Apparent resistivity and phase response curves as a function of period were generated for the LMT site in the north-south (XY) and east-west (YX) directions and were merged with co-located broadband data. The data quality is excellent with smooth response curves and low error bars to periods up to 1,000 s (Figure 3a).

Broadband (BBMT) data were collected at a total of 16 site locations, including the co-located long period site using a combination of MTU-5 and MTU-5a Phoenix Geophysics recording instruments and sensors. The two horizontal perpendicular magnetic field components were recorded using MTC50 Phoenix coils, and the vertical fields were recorded using either a MTC30 or a MTC80 Phoenix coil. Data were collected for at minimum of 22 hours up to a maximum of 3 days, with the exception of 1 site (site dmn218) where a setup error resulted in only 3 hours of data (Table 1). The BBMT data were processed from time series to response functions using robust remote reference techniques (Method 6 in Jones et al., 1989), as implemented by the Phoenix Geophysics software package MT2000, and yielded high quality apparent resistivity and phase response curves in the period range of 0.004 – 1,000 s for most sites (Figure 3b and 3c). Plots of all sites recorded are shown in Appendix I.

Data analysis

Decomposition Analysis

Groom-Bailey decomposition analysis was undertaken in order to understand the degree of dimensionality, determine the most appropriate geo-electric strike direction (where the data are 2-dimensional), and ascertain and remove the effects of galvanic distortion in the data (Groom and Bailey, 1989). Single site decompositions were applied to each of the 2012 MT sites using the method described in McNeice and Jones (2001). The transverse electric (TE) mode refers to data that are parallel to the geo-electric strike direction, and the transverse magnetic (TM) mode refers to data that are perpendicular to strike. In period bands where the phase difference between the TE- and TM-modes is minimal (<10°) the data can be considered to be quasi 1-dimensional (1-D), or independent of the geo-electric strike angle. Where the phase difference is larger, models of the subsurface are strongly dependent on direction and need to be inverted at the appropriate geo-electric strike angle so that they accurately represent the subsurface conductivity structure beneath a profile. Ideally a model can be generated along a profile at one strike angle for all periods. Where the subsurface structure is complex and this angle varies along profile or with depth, the data may need to be divided into sections and modelled separately at the different geo-electric strike angles.

The strike directions resulting from single site, single decade period band decompositions with the 90° ambiguity inherent in the analysis, and an error floor set to 3.5% (equivalent to 2° phase) are shown in figure 4. At periods lower than 0.01 s most of the sites show low phase differences with few exceptions, suggesting that, locally, the near-surface structure is predominantly 1-D.

Strike analysis for the new 2012 data along profile 1 indicate that, with a few exceptions in the northwest and the southeastern most site, the data are predominantly 1-D to periods of 10s (Figure 4). At periods greater than 10 s, data that is likely sensitive to the upper mantle, the phase difference between the two modes is still small (< 15%), however the strike angle at each site is fairly consistent, ranging from 54-65 ° for most of the new sites to 80 – 84° for the southeastern 3 most sites along profile 1. As described in Spratt et al., (2012), analysis of the 2011 data showed that a preferred strike of 68 – 75° is prevalent at periods of 0.01 – 0.1 s in the vicinity of the Committee Bay greenstone units suggestive of near surface structure. The northwestern most sites showed a strong preference of 33° - 47° at periods between 0.1 and 10 s indicative of two-dimensional structure in the lower crust or upper mantle that is not present along the rest of the profile.

Plots of phase differences and strike directions along the northern half of profile 2 (the 2011 data), indicate low phase differences (<10°) for most of the sites at most of the periods, suggesting that the data are predominantly 1-D (Figure 4). The middle section of profile 2 shows a preference of 68 – 72° from 0.01 to 1 s and a weak preference (15% phase difference) of 27 – 33° at periods of 10 – 100 s. The southernmost 2 or 3 sites show a strike direction of 7 – 15° at periods greater than 1s, this change may mark the boundary between Rae domain to the north and the Hearne domain to the south. Among the entire data set, phase differences of approximately 20° are unique to the southern most 2 sites and the off-profile site (dmn222) at periods greater than 10 s. This suggests a difference in the underlying mantle between the Rae and the Hearne domains.

In order to illustrate where the data are sensitive to changes in the strike angle and to determine the angle that is most appropriate for all the data along each profile, the RMS (root mean squared) misfit values from the Groom-Bailey decomposition analysis for each site have been plotted against increasing periods for 4 different strike angles along each of the profiles (Figures 5 and 6). A misfit value of < 2 indicates that a 2-D model of the earth at that strike angle could be adequately represented by the data. Where the misfit value is < 2 regardless of the strike angle, the data can be regarded as 1-dimensional and where the misfit value is systematically > 2 at any geo-electric strike angle indicates possible 2- or strong 3-D distortion effects, an indication that 2-D modelling cannot resolve the subsurface structure and that 3-dimensional modelling is required.

The data along profile 1 were decomposed at strike angles of 84°, 75°, 60°, and 45° (Figure 5). Analysis of the 2011 data showed the preferred geo-electric strike direction of 45° (Spratt et al., 2012). The geo-electric strike angle that best fits most of the sites over most of the period ranges for the entire profile is again 45°, however for the 2012 data, the southeastern half of the profile, a strike angle of 84° is preferred. Several of the sites show high misfit values at all strike angles at the shortest periods (marked by red ellipses in figure 5), indicating localized 3-D distortion effects. These periods have been removed from the data set prior to initiating 2-D inversions. Two-dimensional models have been generated along the entire length of profile 1 with the data recalculated at a strike angle of 45° and the southeastern most sites have been modelled independently at 84°.

Along profile 2, the data were decomposed at strike angles of 10°, 15°, 45°, and 75° (Figure 6). Analysis of the 2011 data showed a general preference of 45° at periods greater than 10s and a strike angle of 75° periods below ~1 s (Spratt et at., 2012). Together with the 2012 sites, the data appear to be independent of strike, or 1-dimensional, through the central part of the profile. The new 2012 data, the

southern half of the profile, show the geo-electric strike angle to be ~15° particularly among the southernmost 3 sites at periods greater than 10 s. Two-dimensional models have been generated along the entire length of profile 2 with the data recalculated at a strike angle of 45° and 15° in order assess features in the models that may be affected by a change in strike angle and the 2012 data have been modelled independently at 15°.

In order to resolve the 90° ambiguity inherent in the strike analysis the sites have been plotted with the regional geology (Figure 2), aeromagnetic data (Figure 7), and bouguer gravity anomalies (Figure 8). In general there is a northeast-to-southwest trend among the northwestern and northern half of the survey area, consistent with a geo-electric strike direction of 45° and identifying the TE-mode direction (parallel to strike). A strike direction of 85° observed in the southeastern half of profile 1 may be related to the east-west trending Wager shear zone, suggesting that this is a major feature extends deep beneath site dmn210, and identifying the TE-mode. The STZ has a strike of approximately 105° where it is crossed by profile 2 and is likely influencing the geoelectric strike angle, suggesting that the TE-mode runs at 105° and the TM-mode at 15°.

Depth estimates

Penetration depths of the measured data in both the xy and yx directions, beneath each site along profiles 1 (Figure 9a) and 2 (Figure 9b) were roughly estimated using Schmucker's c-function analysis, which calculates the depth of maximum eddy current flow (Schmucker, 1970). These estimates indicate that the data at most of the sites along profiles 1 and 2 penetrate to > 200 km depths in at least 1 mode, and in some cases to > 350 km, sufficient for imaging the deep lithosphere of the Earth beneath each profile.

Ocean effects

The presence of sea water can have significant effects on MT data, due to the sharp contrast in resistivity between the land and the ocean (Schmucker, 1970, Menveillie et al., 1982). The coastal effects are typically observed in the long period data and the severity of these effects is dependent on the salinity of the sea water, the conductivity structure of the subsurface, the depth of the ocean, and the proximity of the MT site to the coast (eg. Santos et al., 2001 and Pous et al., 2003). In order to assess the coastal effects on this data set, a 3-D mesh was created with ocean resistivity values of 0.3 ohm-m

extending to depths between 50 and 500 m, (approximated from the International Bathymetric Chart of the Arctic Ocean: http://www.ngdc.noaa.gov/mgg/bathymetry/arctic/arctic.html), and a uniform land resistivity values of 1000 ohm-m (Figure 10a). A forward inversion then calculates synthetic response curves at the recorded site locations. This method of determining coastal effects is a rough guide as the coast line is not exact, the depth and resistivity of the ocean water is approximated, and a uniformly resistive earth was used rather than a layered or structured earth. It is therefore only used to illustrate caution in interpreting 2-dimensional models that include long period data near the coast.

The calculated response curves indicate that effects of the ocean on the 2012 data are minimal with sites nearest to sea water showing minor resistivity and phase changes at periods > 100 s (Figures 10b, c, and d). Depth analysis of site DMN210 shows that a period of 100 s in the XY mode (the recorded north-south direction) corresponds to depths of < 250 km, and site DMN205 in the YX mode to depths of ~ 450 km. This indicates that these data should be able to resolve conductivity features in the crustal and upper mantle.

Data Modelling

The distortion-corrected, regional 2-D responses from sites along the 2 profiles described above have been imported into the WinGlink MT interpretation software package. Each site has been manually edited to remove data points with large error bars or large scatter. Additionally data that were shown to have high misfit values, primarily data in the shortest period range, in the decomposition analysis were removed. Where one apparent resistivity curve of one mode was much higher than another, the curve was dropped to match that of the other curve at the shortest period. This helps to reduce the effect of anisotropic shift, but does not account for the static shift cases were both curves are affected.

1-D Models

One-dimensional layered earth models were generated for each site in both the TE and TM-modes using Occam's inversion codes as implemented by the WinGlink MT interpretation software package and were stitched together to form cross-sections along the 2 profiles (Figures 11a and 12a). Pseudosections of the phase responses for each of the sites along profiles 1 and 2 were generated for both the TE- and TM-modes (Figures 11b and 12b). Where these sections are similar, the 1-D models

can be considered to be a valid representation of the Earth. Along profiles 1 and 2, the data can be regarded as 1-D only for the shortest frequencies, to depths of approximately 10 km (Figures 11 and 12).

2-D Modelling

The WinGlink™ interpretation software package that implements Rodi and Mackies (2001) inversion algorithm was used to generate two-dimensional models along profiles 1 and 2. Inversions were executed from the distortion corrected responses re-calculated at the appropriate geo-electric strike direction. The inversion program searches for the smoothest, best-fit model with the least deviation from the starting model (Mackie and Madden, 1993). The models derived represent the minimum structure required to fit the data with an acceptable misfit.

In order to determine the most appropriate smoothing value (tau), several models were generated using data from the entire period range of 0.004 – 10,000 s in both the TM- and TE-modes. The error floor was set to 25% for the apparent resistivity to account for static shift effects, and 7% for the phase. For each model tau was changed after 100 iterations and the final RMS for each run was recorded. Figure 13 illustrates the trade-off between the roughness of the models (defined by the tau parameter) and the fit of the model to the data (the RMS value). These plots indicate that a tau value of 3-5 would result in the smoothest model with the best fit to the data along profile 1, a value of 3 would be appropriate along profile 2.

Models were generated along each profile using different components of the data at the various strike angles in order to assess the change in the observed conductivity structure. At periods where high RMS values were observed in the decomposition analysis (figures 5 and 6), the data were omitted from 2-D modeling. The inversions were initiated with a homogeneous half space of 500 ohm-m, the phases were set with a 2° error floor, and where applicable, the Tipper error was set to an absolute value of 0.01. Initially the apparent resistivities were set with an error floor of 25%, and subsequently reduced to 7% to assess and account for static shift effects.

Preliminary 2-D models

Profile 1

Preliminary two-dimensional models of the MT data along profile 1 have been generated at a strike of 45° (Figure 14), using the TM and TE-modes from all sites with an apparent resistivity error

floor of 25% (Figure 14a), using the TM and TE-modes from all sites with an apparent resistivity error floor of 7% (Figure 14b), and using the TM, TE-modes, and the Tipper data from all sites with an apparent resistivity error floor of 25% (Figure 14c). The northwestern half and southeastern half of profile 1 were modelled independently at 45° (Figure 14d) and 84° (Figure 14e) respectively using data from the TM and TE-modes with an apparent resistivity error floor of 25%. The models are similar to depths of ~100 km suggesting that static shift effects in the data are minimal.

The models reveal a resistive crust (> 10,000 ohm-m) extending to 30 – 40 km depths that is underlain by a discontinuous less resistive (500 – 2000 ohm-m) layer. The upper mantle beneath most of the profile is shown to be resistive (>8000 ohm-m) to depths of 180 - 220 km, below which there is a decrease in resistivity values (< 1000 ohm-m) that is interpreted as the lithosphere-asthenosphere boundary. The models reveal a less resistive zone at depths of 50 – 150 km beneath the northwestern-most extent of profile 1.

Some significant differences are observed between the various models, particularly at depths greater than ~100 km. All of the models show a less resistive upper mantle (ranging from 300 – 1000 ohm-m) at depths of 50 – 150 km beneath the northwestern-most extent of profile 1. This change from northwest to southeast is consistent with changes observed in the strike analysis (Figure 4) to periods of 10 s. The specific location, orientation, and conductivity value varies significantly between the models. Model testing and further focused inversions may be required to resolve this feature. Another inconsistent feature is the depth to the lithosphere-asthenosphere boundary, which ranges from ~180 km in figure 14a, to ~220 km in figure 14b.

Structural features are imaged within the crust beneath profile 1 (Figures 14d and e): a) a mid-lower crustal conductor (10 – 100 ohm-m) is imaged beneath site DMN104, b) the conductive lower crust observed throughout the region is discontinuous to the northeast of this conductor as well as in the vicinity of site DMN216, c) the lower crustal conductor appears to extend towards the surface on either side of site DMN216 where the upward trend to the southeast may mark the near surface expression of the Wager Bay shear zone, and d) the mid-lower crust shows moderate conductivity values (100 – 1000 ohm-m) beneath the southeastern-most extent of the profile. Modelling of the high frequency data alone may be able to further resolve these structures.

Profile 2

Models have been generated along profile 2 at a strike of 45° (Figure 15) and at a strike of 105°

(Figure 16), using the TM and TE-modes from all sites with an apparent resistivity error floor of 25% (Figures 15a, and 16a), using the TM and TE-modes from all sites with an apparent resistivity error floor of 7% (Figures 15b and 16b), and using the TM, TE-modes, and the HZ data from all sites with an apparent resistivity error floor of 25% (Figures 15c, and 16c). The northern half of the profile (the 2011 data) and the southern half of the profile (the 2012 data) have been modelled separately at strike angles of 45° (Figure 16d) and 105° (Figure 14e) respectively. All of the models reveal similar features with some variation.

The models generated at 45° and at 105° show very similar structure beneath the northern-most extent of profile 2, consistent with previous interpretations of a 1-D earth. Beneath the southern half of the profile, the lower crustal conductive layer is imaged as 'spotty' in the models generated at a strike of 45°. This suggests that the data have been modelled at an inappropriate strike angle and that the models generated at 105° are more appropriate. Beneath site DMN119, the lower crustal conductive layer is discontinuous when modelled at 45°, but continuous at 105°. Plots of RMS values from decomposition analysis (Figure 16) showed that site dmn119 did not fit a strike of 15°, but that 45° was preferred suggesting that the models at this strike are more accurate and that the discontinuous lower crustal conductor beneath this site is a true feature.

At depths up to 100 km the models are very similar showing a resistive layer that ranges in thickness from 15 to 40 km along the profile, likely Archean orthogneiss in the crust. This resistive material is underlain by a less resistive lower crustal layer (~1000 ohm-m) that varies in depth and thickness and is discontinuous in the vicinity of site DMN208 and DMN119. This less resistive layer appears to extend towards the surface in the vicinity of site DMN207 and may mark the location of the Snowbird Tectonic Zone (Figure 16d). Similar to profile 1, a mid-to-lower crustal conductor (< 100 ohm-m) is imaged beneath site DMN111 that lies along strike from that found beneath DMN104. Both of these locations (along profiles 1 and 2) correlated with a change in the regional bouguer gravity signature (Figure 8) and may represent structure that separates granulite facies orthogneiss from lower grade Archean crust.

Beneath most of profile 2, the upper mantle lithosphere is consistently imaged as resistive (>50,000 ohm-m) to depths of 200 – 220 km. Towards the south end of the profile, these resistivities decrease to ~10, 000 ohm-m, possibly marking the boundary between the Rae mantle lithosphere to the north and the Hearne mantle to the south. Although the orientation and specific resistivity value varies between models, there is a consistent decrease in resistivity beneath site DMN217 that extends through

to at least 200 km (Figures 16a, b, and c). Model testing should be undertaken to ascertain the robustness of this feature. At depths below 200 – 220 km all of the models show an decrease in resistivity interpreted as the lithosphere-asthenosphere boundary.

Figure 16e shows the 2-d model of the northern half of profile 2 inverted from data recalculated at 45°. After over 200 iterations, values of ~1000 ohm-m were observed at upper mantle depths. Subsequently, a resistive layer was inserted between 50 – 220 km and a less resistive layer at depths greater then 220 km, a structure that is consistent with the whole profile models. A further 100 iterations showed little change from the altered model, suggesting that the data may not be sensitive to structure at these depths and model testing is required.

Conclusions

Careful processing and analysis of the 2012 Diamonds MT data collected have provided a good understanding of dimensionality and distortion of the data, and show that the quality of the data is sufficient to model the lithospheric conductivity structure. Decomposition analysis indicates that the geo-electric strike angle varies across the region and that, in general, a 2-D representation of the subsurface conductivity structure beneath profiles 1 and 2 is reasonable. Modelling of the data at different strike angles using different variables has helped to determine some of the inversion parameters that should be used to provide an accurate image of the subsurface. Preliminary 1-D and 2-D models reveal some structure that appears to be consistent in the data. These models also illustrate the need for additional 2-D and 3-D inversions, which are required to further resolve the subsurface conductivity structure. In general a resistive crust is underlain by a discontinuous less resistive lower crust. Structural features are observed in the crust that may be related to major regional shear zones. Some lateral variations are noted within the mantle lithosphere and a decrease in resistivity at depths of 180 – 220 km likely marks the lithosphere – asthenosphere boundary. Hypothesis testing should be undertaken to assess the sensitivity of the data to various features, particularly the deep structure beneath the profiles.

Acknowledgments

This work was funded by Natural Resources Canada. The author would like to acknowledge Azad Rafeek, and Tom Skulski for providing background maps for several of the figures.

References

Groom, R.W., and R.C. Bailey, 1989: Decomposition of magnetotelluric impedance tensors in the presence of local three-dimensional galvanic distortion; Journal of Geophysical Research, v. 94, p. 1913 – 1935.

Henderson, J.R., and J. Broome, 1990: Geometry and kinematics of Wager shear zone interpreted from structural fabrics and magnetic data; Canadian Journal of Earth Science, v. 27(4), p. 590-206, doi: 10.1139/e90-055.

Hoffman, P. F., 1988. United plates of America, the birth of a craton: Early Proterozoic assembly and growth of Laurentia, Ann Rev. Earth, Planet, Sci., v.16, p. 543– 603.

Jones, A.G., Chave, A.D., Auld, D., Bahr, K. and Egbert, G., 1989: A comparison of techniques for magnetotelluric response function estimation; Journal of Geophysical Research, v. 94, p. 14,201 – 14,213.

Jones, A.G., and H. Jodicke, 1984: Magnetotelluric transfer function estimation improvement by a coherence-based rejection technique, paper presented at the 54th Society of Exploration Geophysics Annual General Meeting, Atlanta, George, 2-6 December, Abstract volume, pp. 51-55.

Mackie, R.L., and T.R. Madden, 1993: Three-dimensional magnetotelluric inversion using conjugate gradients; Geophysical Journal International, V. 115, p. 215 – 229.

McNeice, G.W., and A.G. Jones, 2001: Multisite, multifrequency tensor decomposition of magnetotelluric data; Geophysics, v. 66, p. 158 – 173.

Menvielle, M.J.C., P. Rossignal, and P. Tarits, 1982: The coast effect in terms of deviated electric currents: A numerical study; Physics of the Earth and Planetary Interiors, v. 28, p. 118 – 128.

J. Pous, W. Heise, P.A. Schegg, G. Munoz, J. Mart, and C. Soriano, 2002. Magnetotelluric study of the Las Canadas caldera (Tenerife, Canary Islands): structural and hydrogeological implications; Earth and Planetary Science Letters, v. 204, p. 249 – 263.

F. A. M. Santos, M. Nolasco, E. P. Almeida, J.Pous and L.A. Mendes-Victor: 2001. Coast effects on magnetic and magnetotelluric transfer functions and their correction: application to MT soundings carried out in SW Iberia; Earth and Planetary Science Letters, v.186, p. 283-295.

Rodi, W., and R.L. Mackie, 2001: Nonlinear conjugate gradients algorithm for 2-D magnetotelluric inversion, *Geophysics*, v. *66*, p. 174 - 186.

Schmucker, U., 1970: Anomalies of geomagnetic variations in the southwestern United States, Bull. Scripps Ints. Oceanogr. v. 13, 165 p.

Spratt, J.E., Snyder, D.B. and Craven, J.A., 2011: A magnetotelluric survey across the Committee Bay belt and Rae craton in the Churchill province of Nunavut; Geological Survey of Canada, Open File 6825, 28 p.

Spratt, J.E., Snyder, D.B., and Craven, J.A., 2012. Magnetotelluric sounding in the Committee Bay belt, northern Churchill area, Nunavut; Geological Survey of Canada, Open File 7063, 37 p. doi: 10.4095/289836.

Site	Data Range	Latitude	Longitude	Duration of acquisition
dmn222	LMT	63.2987	-92.2928	7 days
dmn204	BBMT	63.4498	-92.9977	22.1 hours
dmn205	BBMT	63.8216	-92.9182	23.1 hours
dmn206	BBMT	64.1051	-92.8490	42.1 hours
dmn207	BBMT	64.4121	-92.6934	67.1 hours
dmn208	BBMT	64.8330	-92.5881	52.3 hours
dmn209	BBMT	65.3321	-92.2806	48.2 hours
dmn210	BBMT	64.6297	-89.4649	45.4 hours
dmn211	BBMT	64.7814	-89.9218	43.0 hours
dmn212	BBMT	64.9289	-90.2493	65.6 hours
dmn213	BBMT	65.0609	-90.6926	43.5 hours
dmn214	BBMT	65.2049	-91.0701	74.0 hours
dmn215	BBMT	65.4045	-91.3154	40.8 hours
dmn216	BBMT	65.5588	-91.6190	50.2 hours
dmn217	BBMT	65.7593	-91.9899	50.2 hours
dmn218	BBMT	65.9095	-92.3534	3.0 hours
dmn222	BBMT	63.2987	-92.2928	36.2 hours

Table 1

Table 1: Site type, location, and recording times for each of the MT sites collected along during the 2011 Diamonds MT field season.

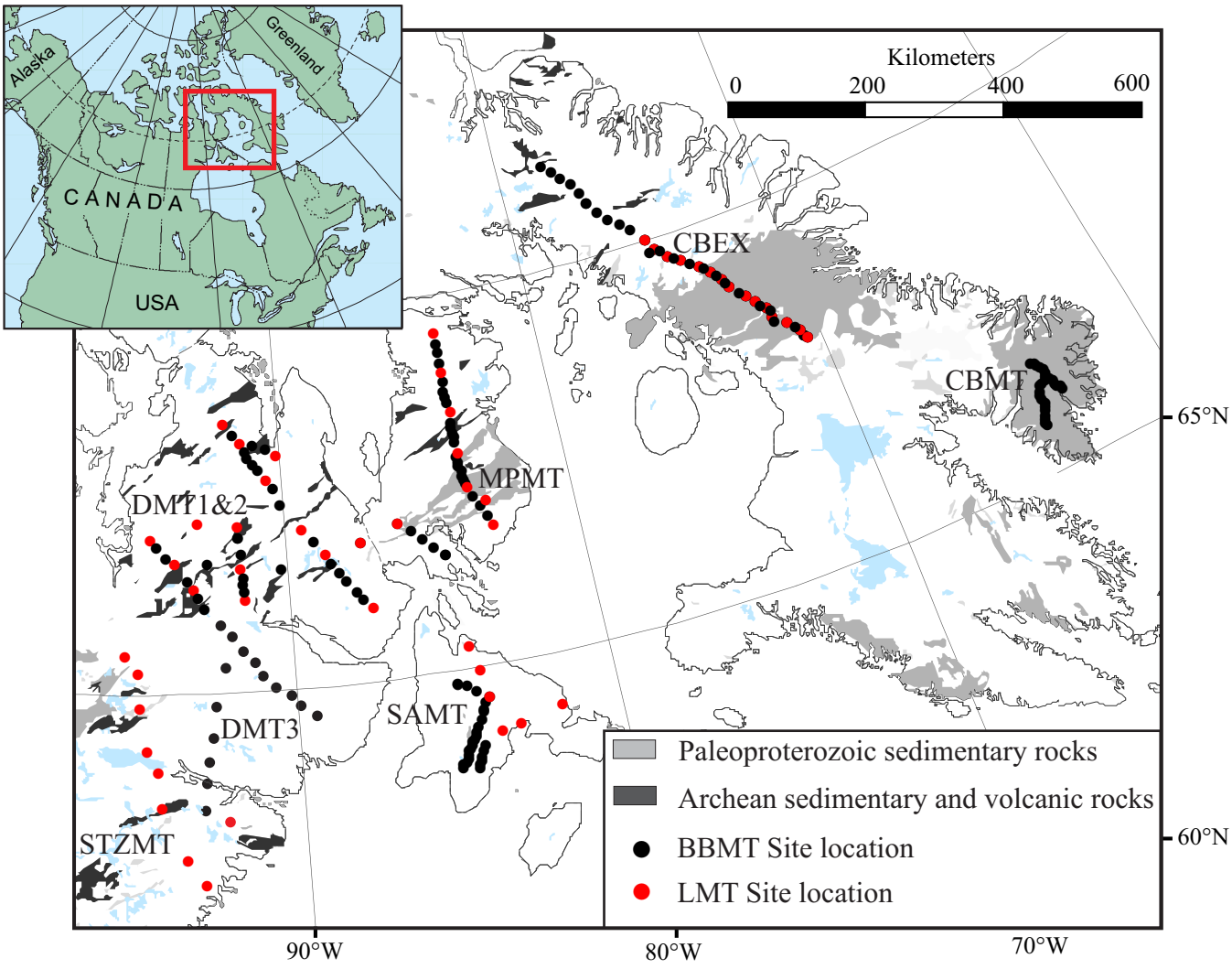

Figure 1: Regional map illustrating the locations of MT surveys in eastern Nunavut: CBEX= the Central Baffin Magnetotelluric Experiment, MPMT = Melville Peninsula Magnetotelluric survey, SAMT = Southampton Magnetotelluric survey, DMT1 = Diamonds Magnetotelluric survey: 2010 data, DMT 2 = Diamonds Magnetotelluric survey: 2011 data, DMT 3 = Diamonds Magnetotelluric survey: 2012 data, CPMT - Cumberland Peninsula Magnetotelluric survey, and STZMT - Snowbird Tectonic Zone Magnetotelluric survey

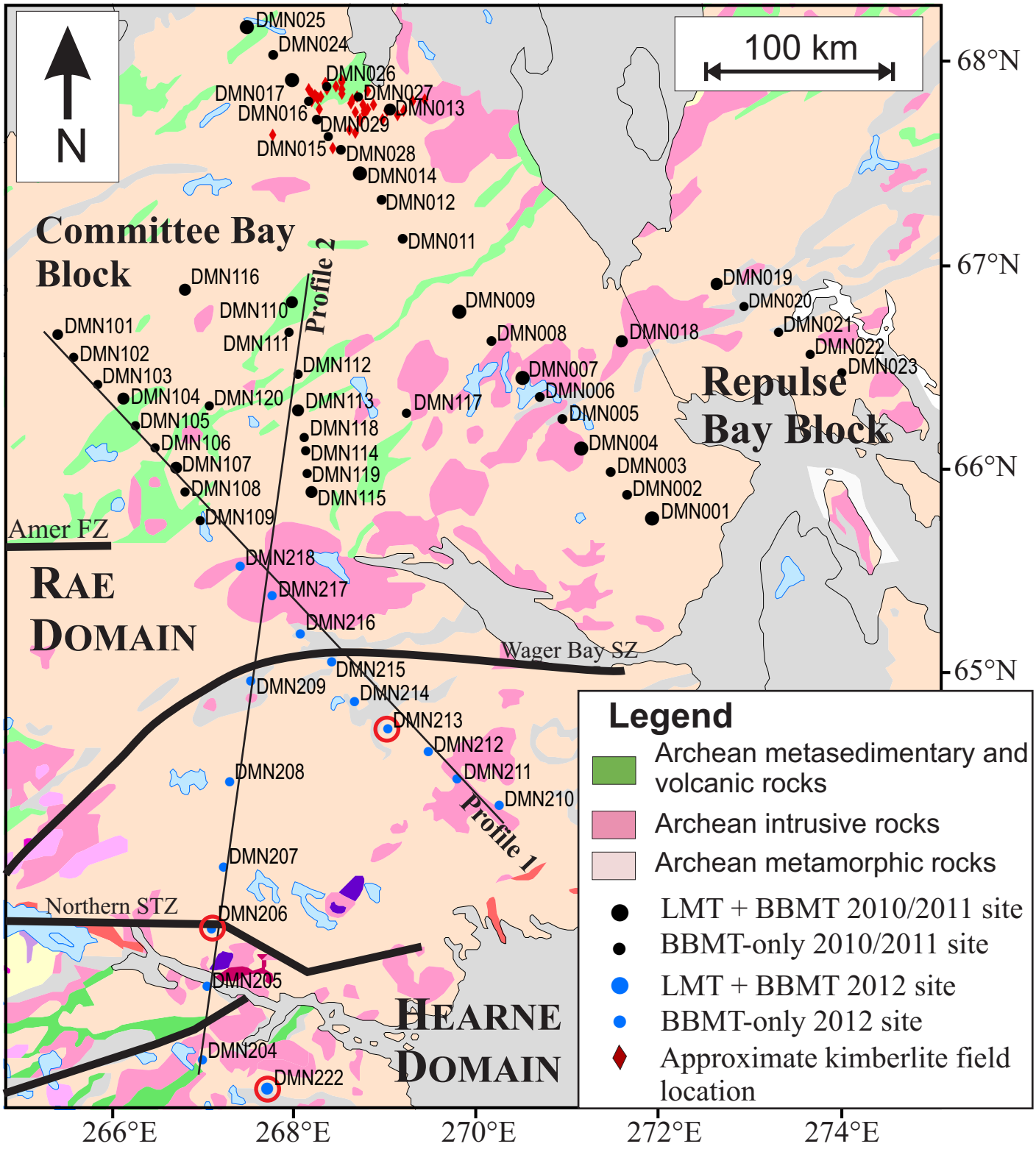

Figure 2: Geological map of the survey area showing the location of the MT sites recorded. The thin black lines mark the profile traces used for 2-D modelling and the red circles mark the location of examples of the response curves shown in figure 3.

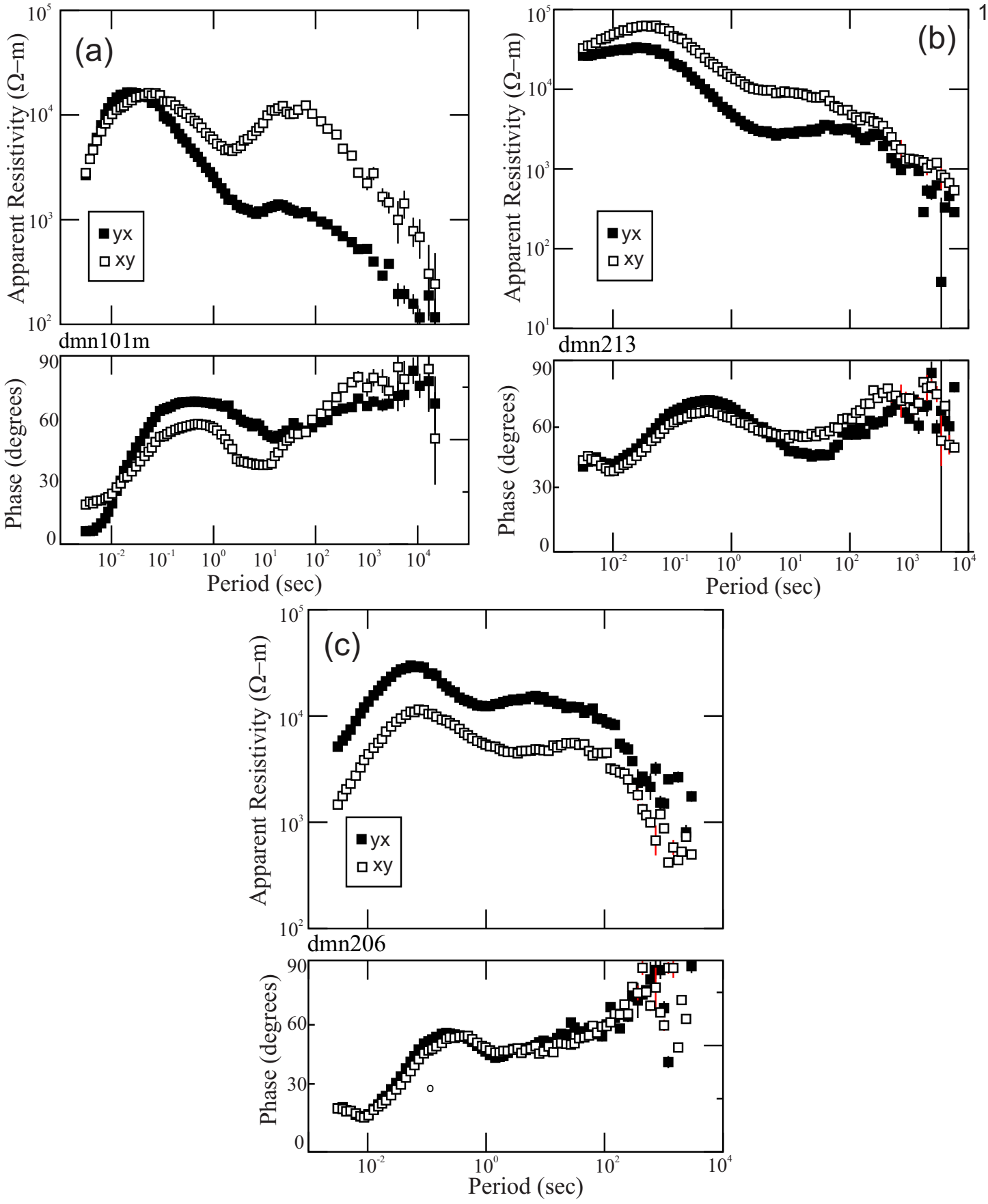

Figure 3: Examples of apparent resistivity and phase MT response curves for data measured at 3 sites: (a) shows merged broadband and long period data at a site located within the Hearne domain, (b) shows an example of the long period data recorded along profile 1, (c) shows an example of the broadband data along profile 2.

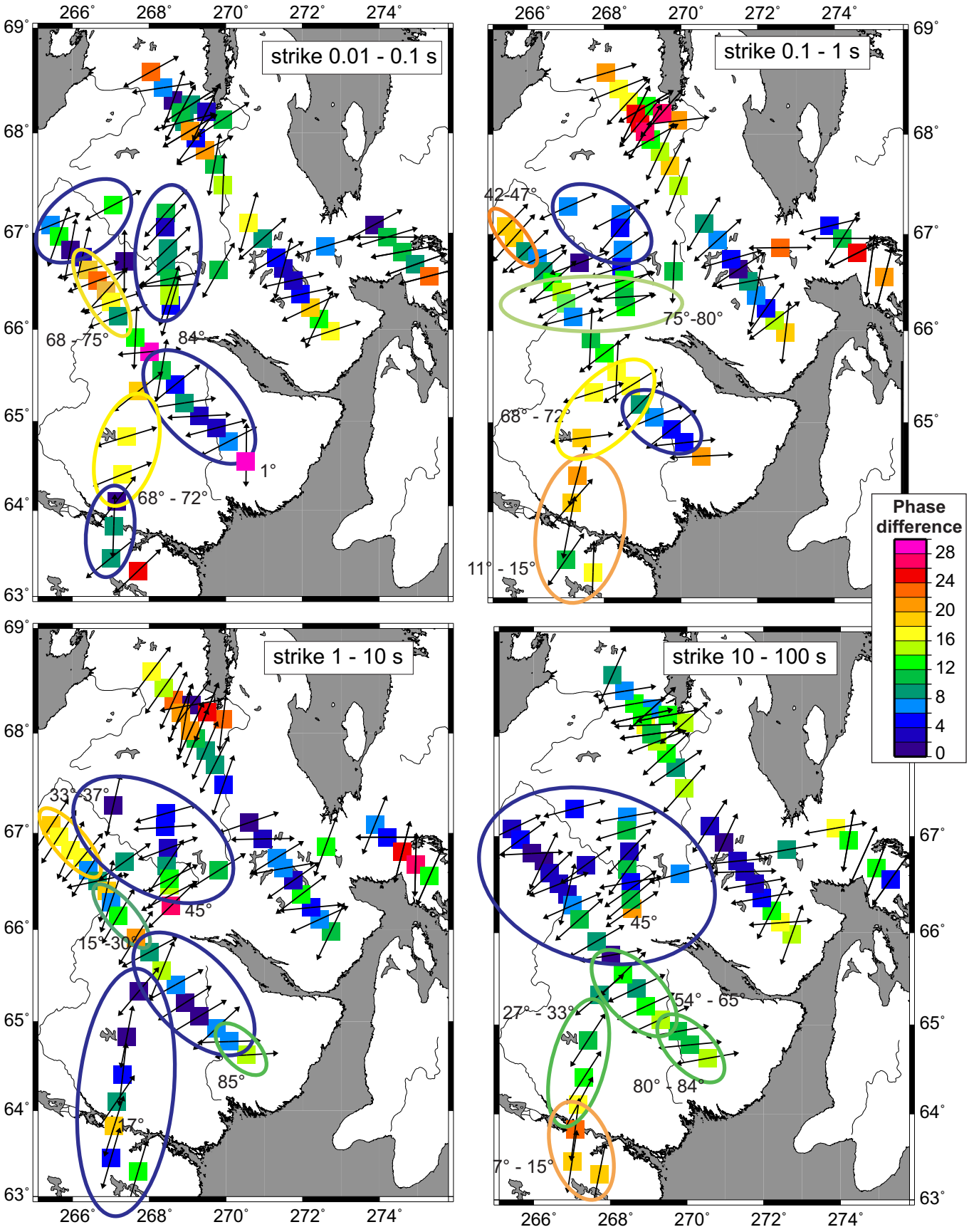

Figure 4: Maps showing the preferred geo-electric strike direction at each site for decade period bands. The color scale illustrates the maximum difference between the TM- and TE-mode phases. The blue ellipses show areas where the data can be regarded as 1-dimensional, the yellow and red ellipses illustrate the location and period range where the model will be most dependent on the geo-electric strike angle.

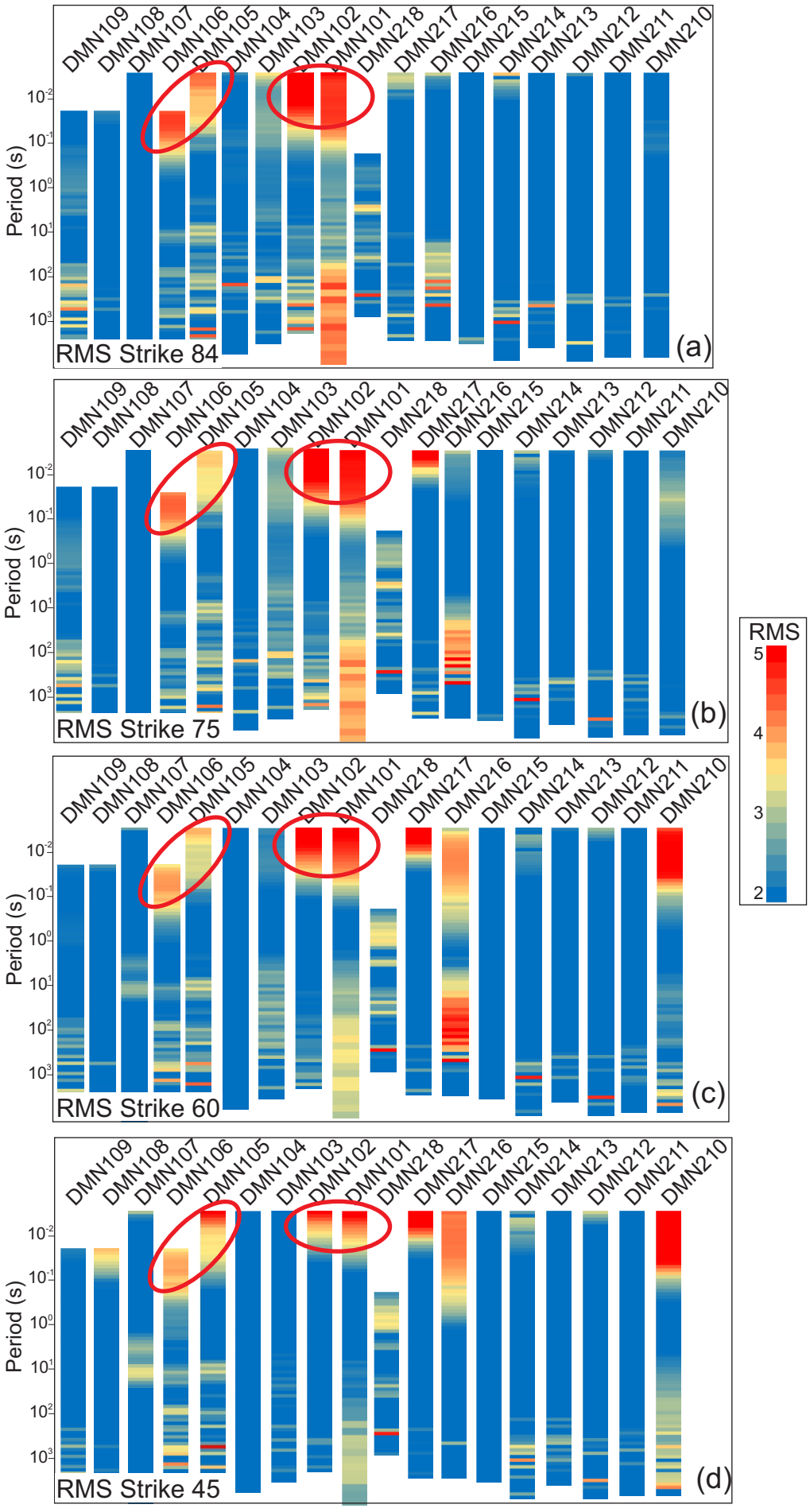

Figure 5: Data misfit values at each site over the whole recorded period range for data along profile 1, recalculated at a geo-electric strike direction of 84° (a), 75° (b), 60° (c), and 45° (d). The red ellipses mark data that have low RMS values at any strike angle.

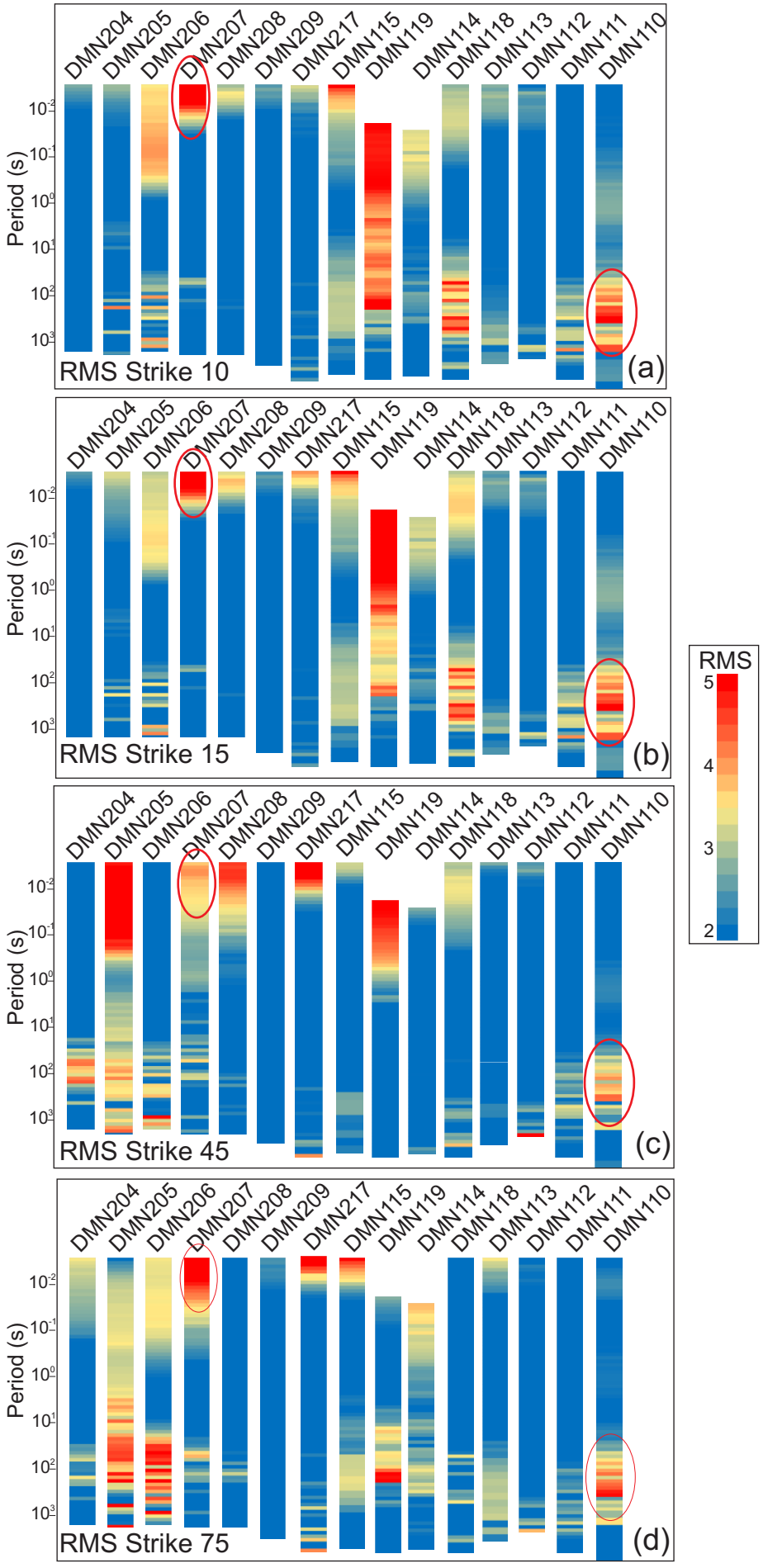

Figure 6: Data misfit values at each site over the whole recorded period range for data along profile 1, recalculated at a geo-electric strike direction of 10° (a), 15° (b), 45° (c), and 75° (d). The red ellipses mark data that have low RMS values at any strike angle.

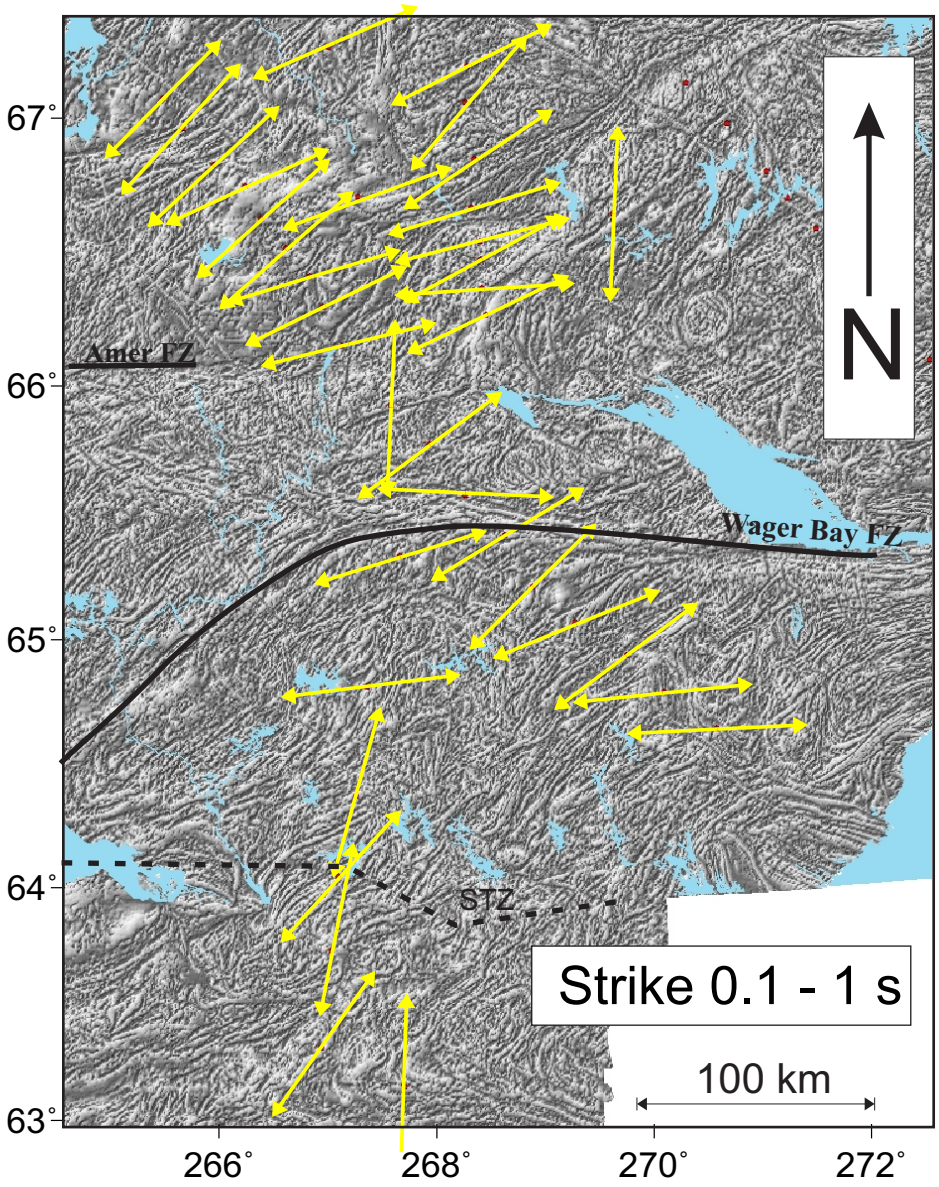

Figure 7: Map of the MT survey area showing the aeromagnetic tilt data. The yellow arrows show the preferred geo-electric strike direction at the 0.1 1 s period bandwidth. The black lines mark major fault zones visible in the magnetic data.

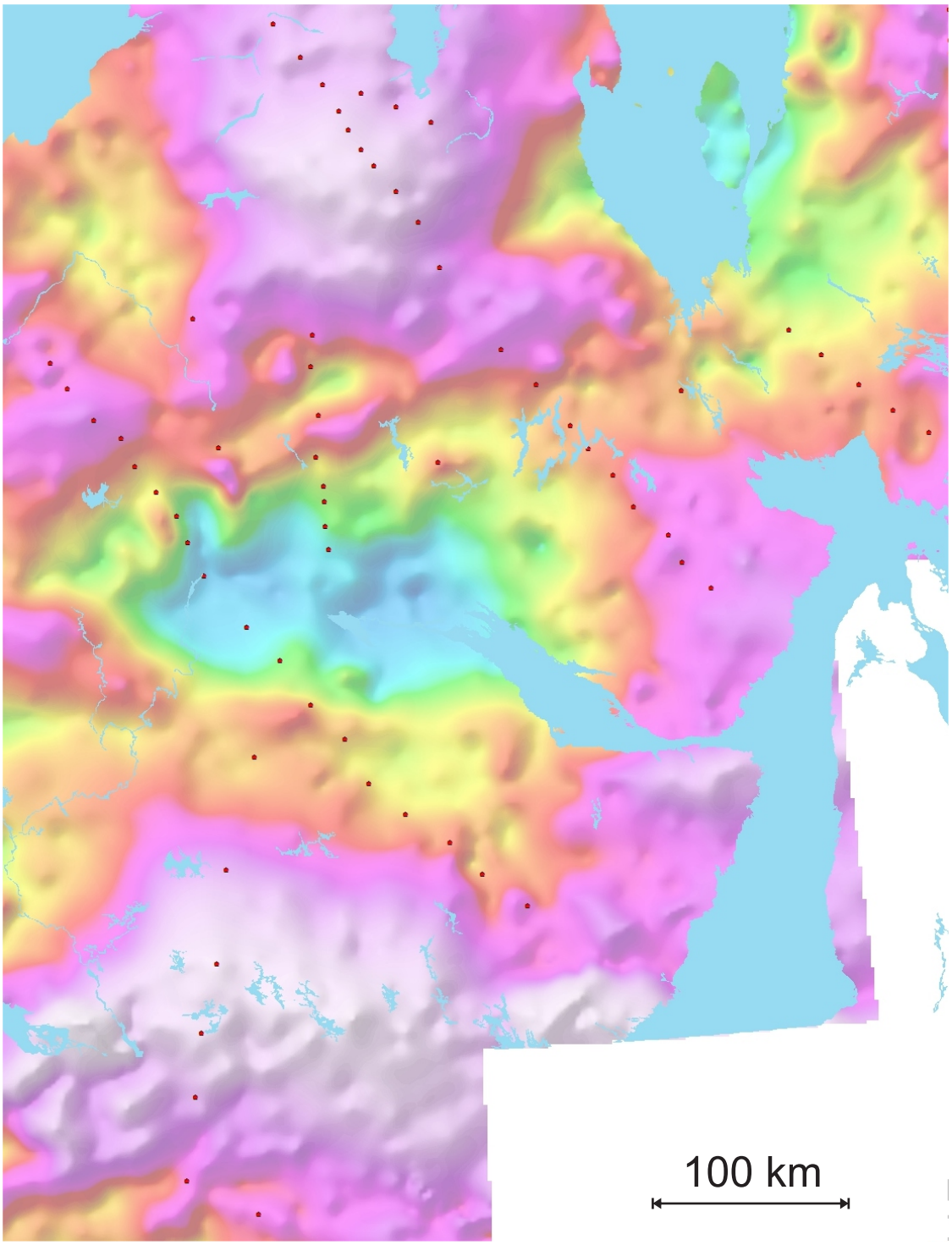

Figure 8: Map of the MT survey area showing the bouguer gravity data

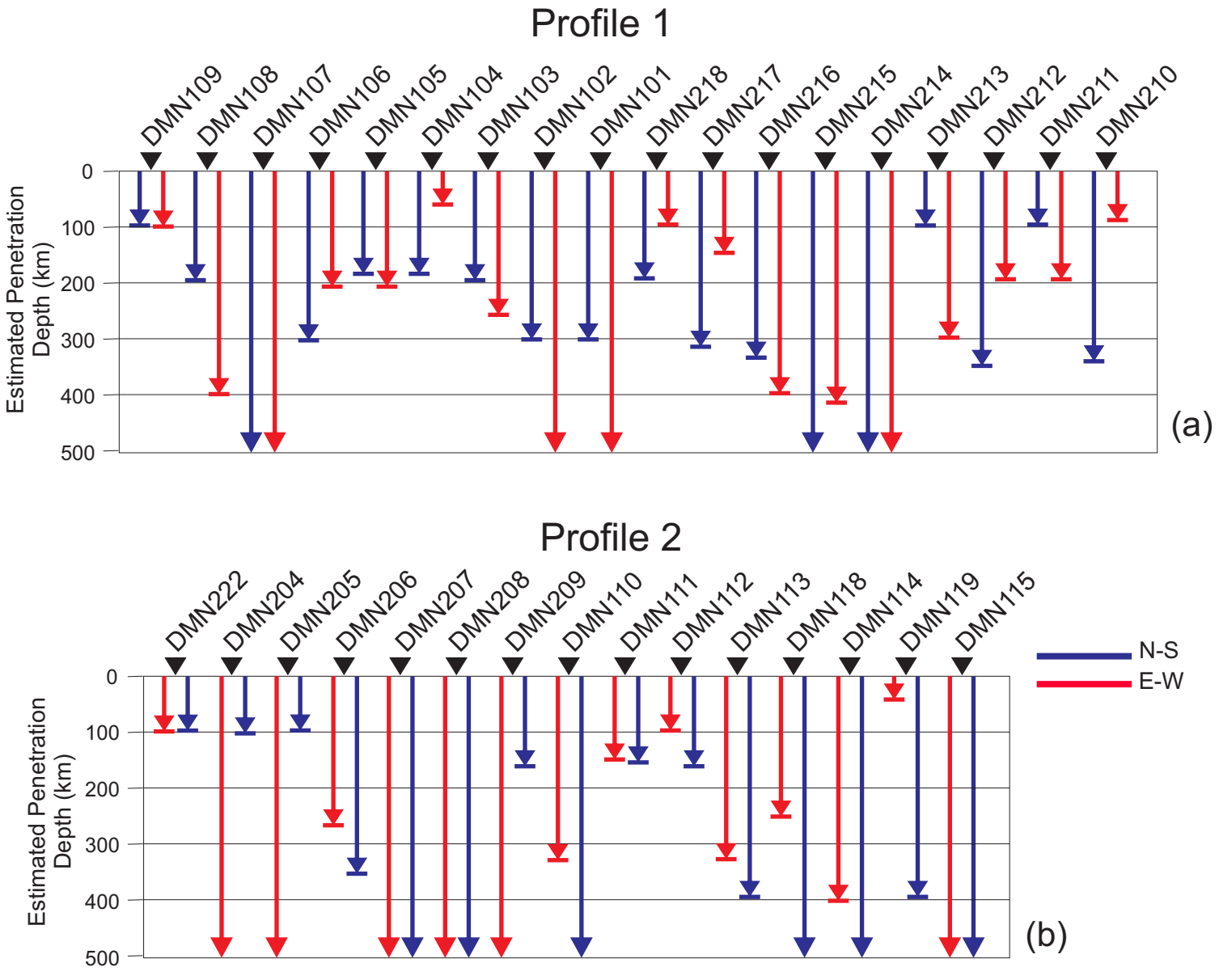

Figure 9: Estimates of maximum penetration depths for each mode beneath each MT site. (a) shows the results along profile 1, (b) shows the results along profile 2.

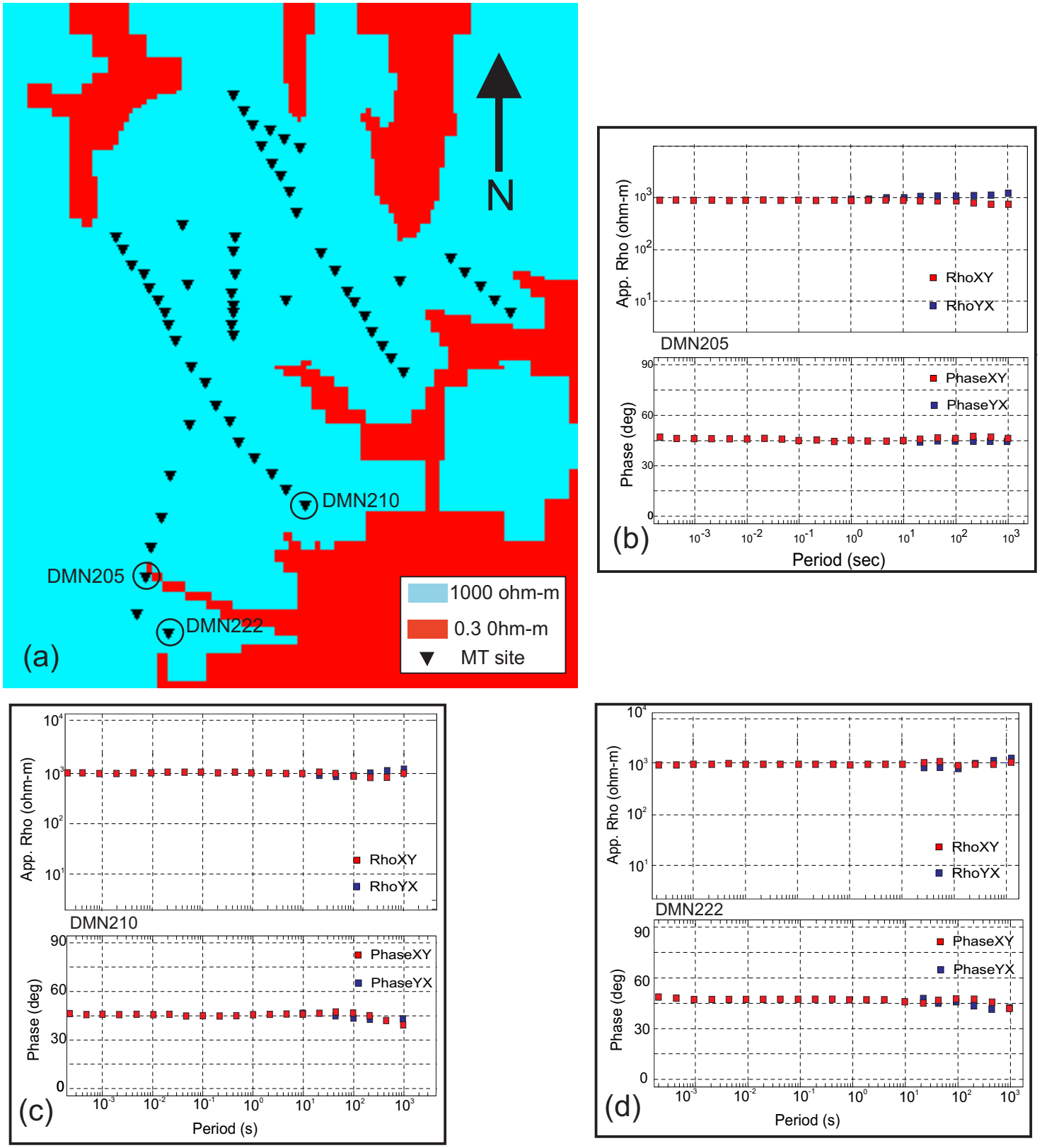

Figure 10: The 3-D mesh of the MT survey area showing the land versus ocean conductivity contrast (a). Examples of the forward calculated response curves are shown for sites DMN205 (b), DMN210 (c), and DMN222 (d).

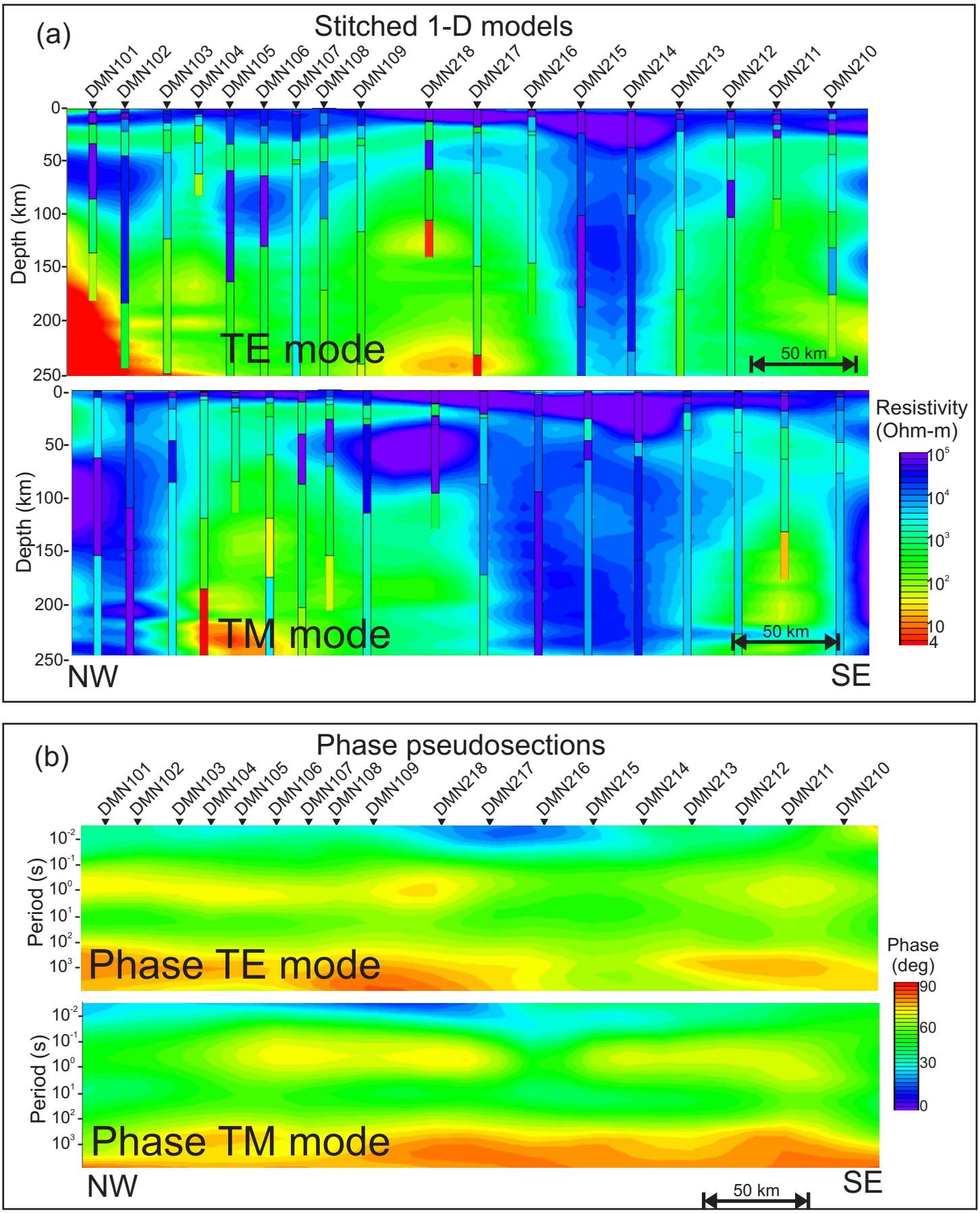

Figure 11: (a) Cross-sections along profile 1, the westernmost profile illustrating the results of 1-dimensional Occam inversions in the TE- (top) and TM- (bottom) modes. (b) Pseudosections along of the phases of the sites along profile 1, with increasing period of both the TE- (top) and TM- (bottom) modes.

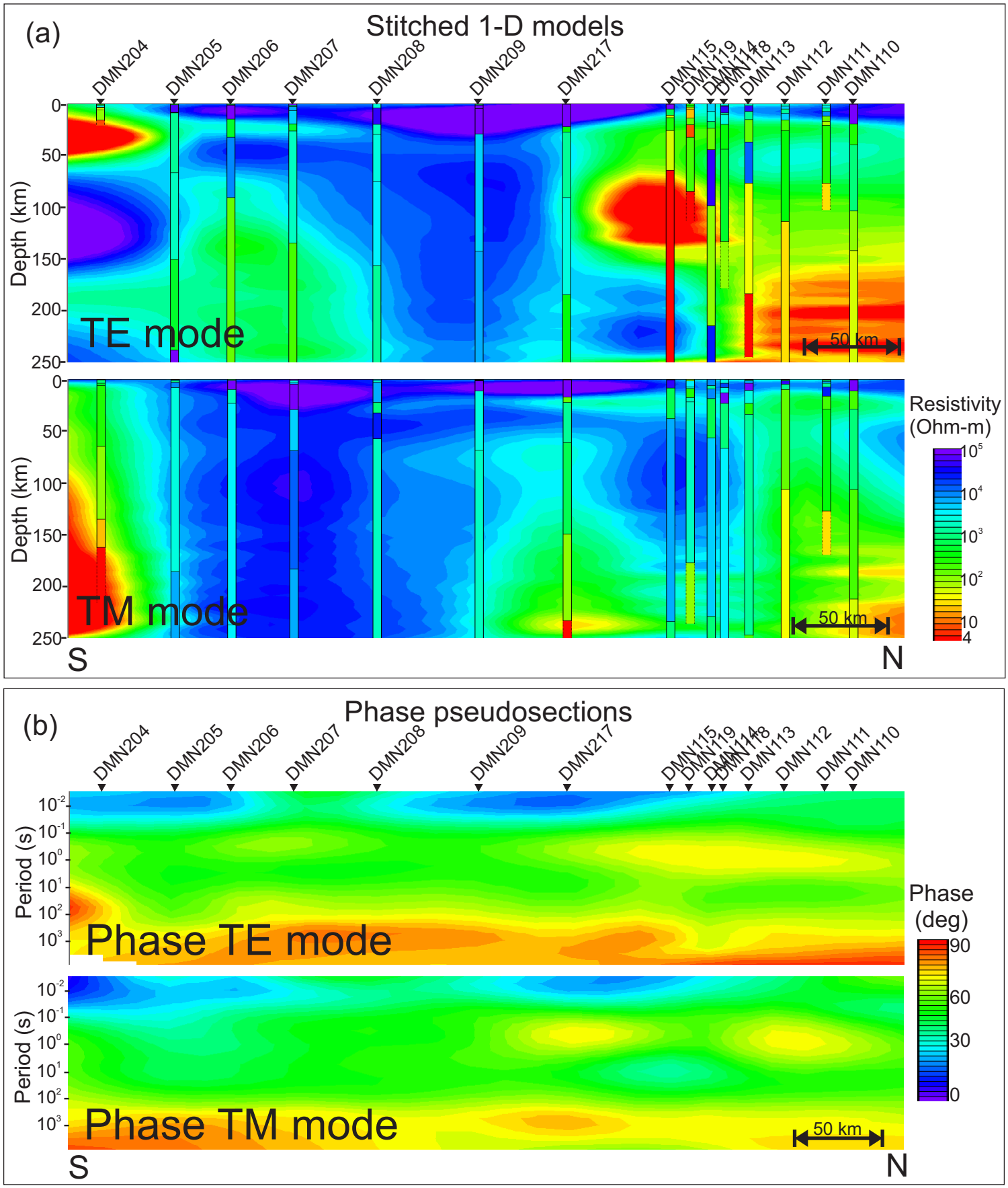

Figure 12: (a) Cross-sections along profile 2 illustrating the results of 1-dimensional Occam inversions in the TE- (top) and TM- (bottom) modes. (b) Pseudosections along the western most profile of the phases of the sites along profile 2, with increasing period of both the TE- (top) and TM- (bottom) modes.

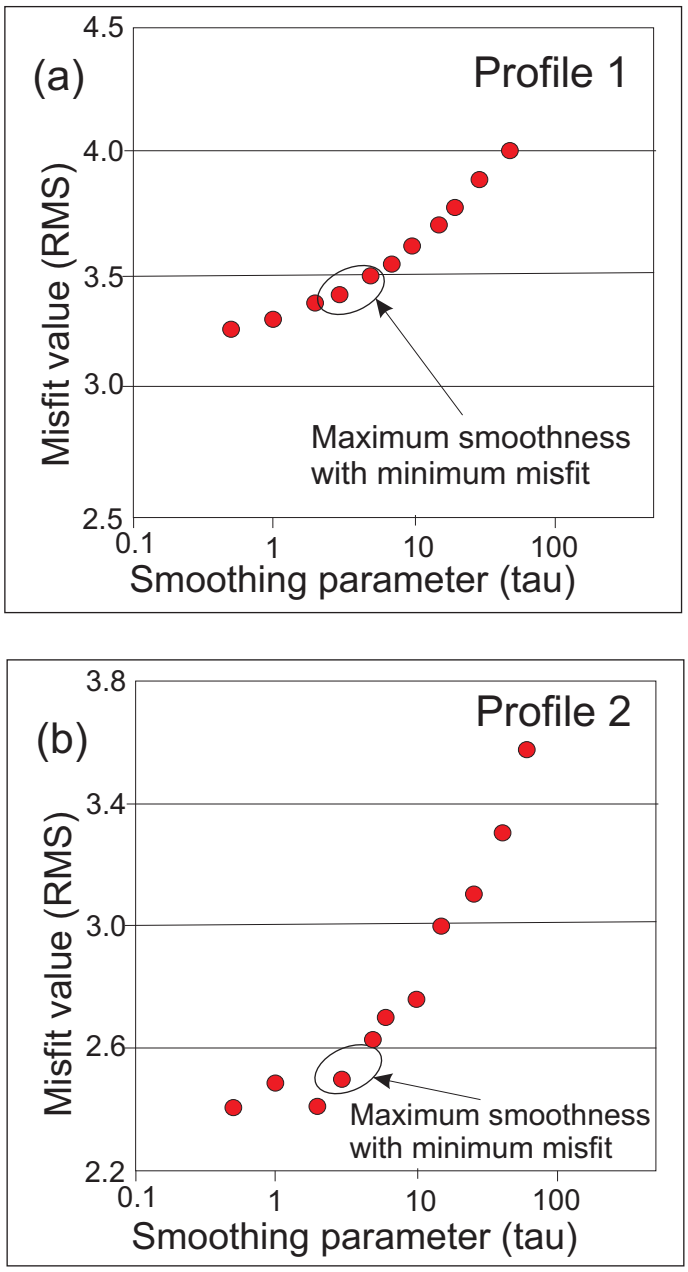

Figure 13: Plots of the trade off between the RMS misfit of the model to the data and the tau value of the inversion. (a) shows the results after 100 iterations along profile 1, and (b) shows the results along profile 2. The black ellipse in each plot marks the optimal tau value for each line.

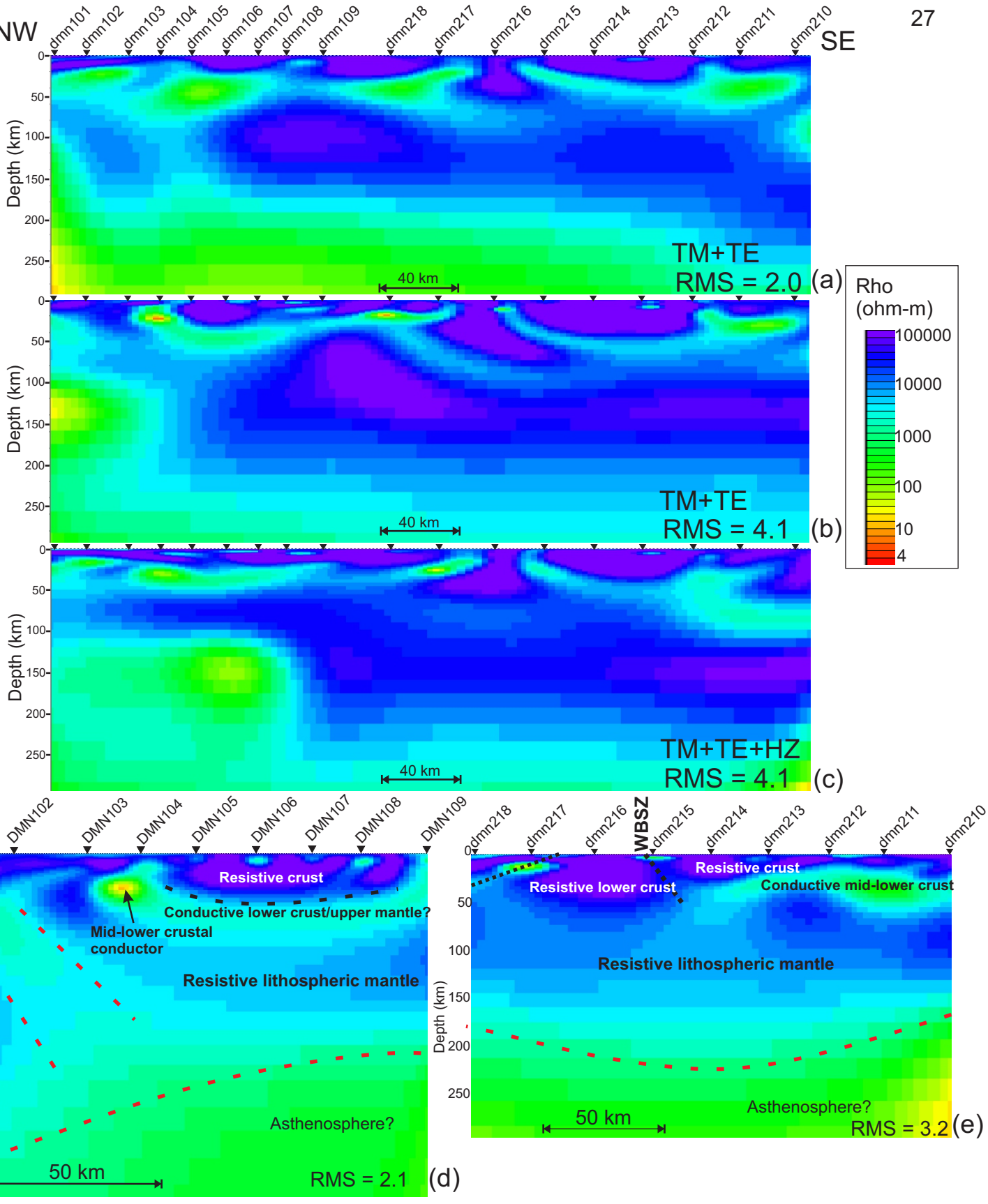

Figure 14: Preliminary model showing the conductivity structure of the lithosphere beneath profile 1, the westernmost Diamonds MT profile. The red colours illustrate areas of low resistivity and the blue colours represent resistive material. Model (a) shows results of inversion using TM and TE-mode data at 45° with high error floors set on the apparent resistivities, (b) shows results using TM and TE-mode data at 45° with lower error floors on the apparent resistivities, (c) shows results using TM, TE, and HZ-data at 45°, (d) shows results of inverting the northwestern most sites using the TM and TE-mode data at 45°, and (e) shows results of inverting the southeastern most sites using the TM and TE-mode data at 84°.

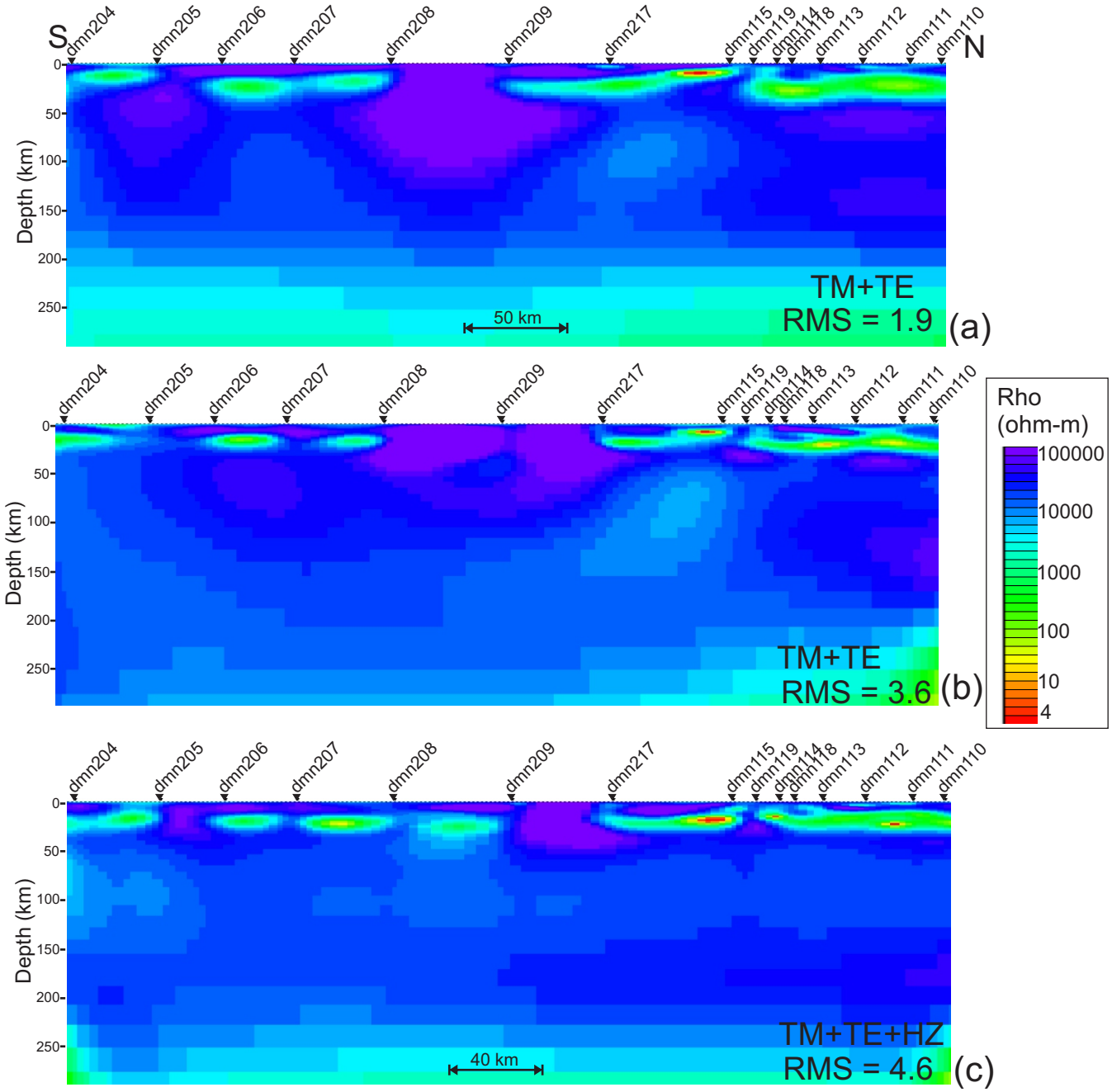

Figure 15: Preliminary model showing the conductivity structure of the lithosphere beneath profile 2, the westernmost Diamonds MT profile. The red colours illustrate areas of low resistivity and the blue colours represent resistive material. Model (a) shows results of inversion using TM and TE-mode data at 45° with high error floors set on the apparent resistivities, (b) shows results using TM and TE-mode data at 45° with lower error floors on the apparent resistivities, and (c) shows results using TM, TE, and HZ-data at 45°.

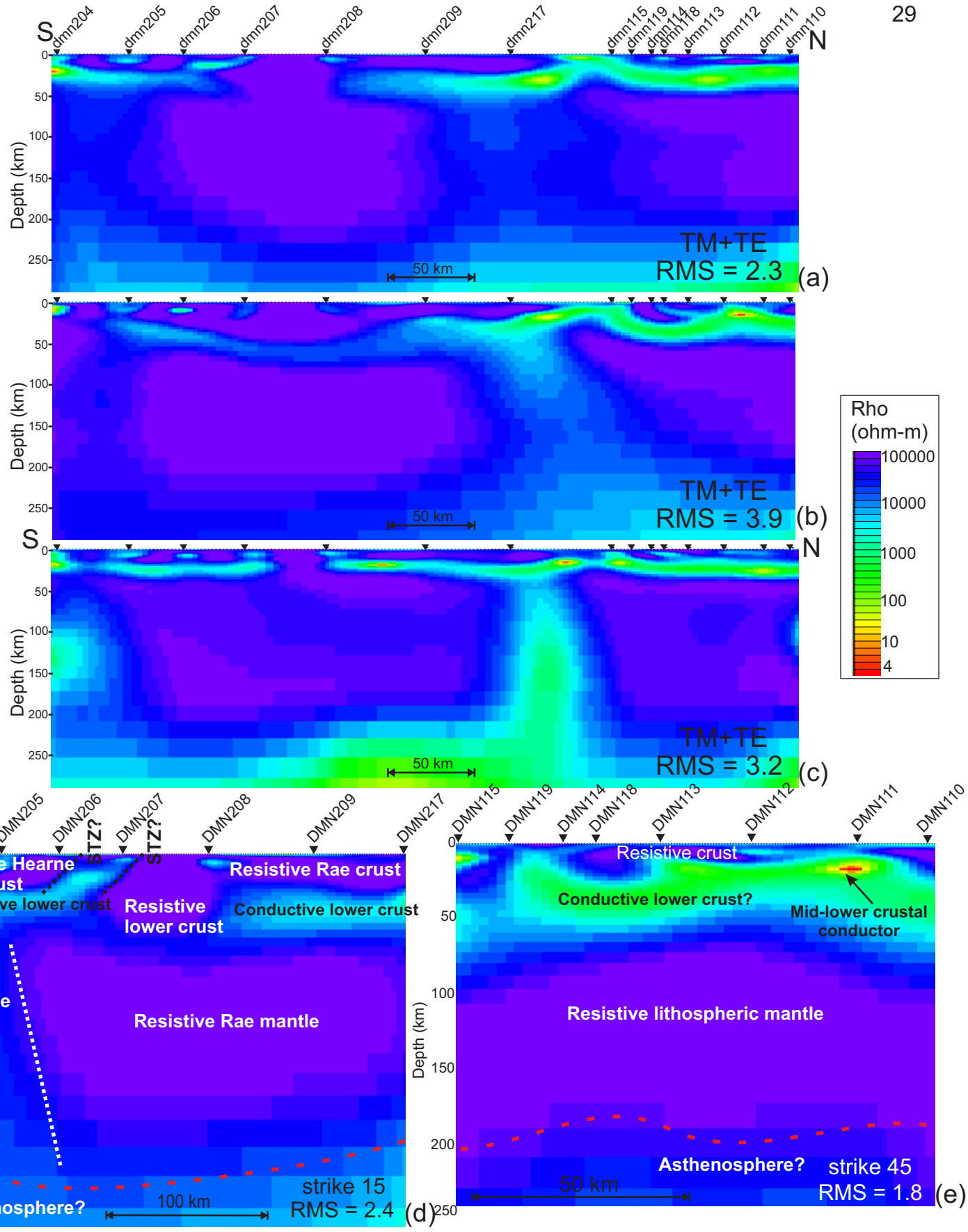

Figure 16: Preliminary model showing the conductivity structure of the lithosphere beneath profile 2, the westernmost Diamonds MT profile. The red colours illustrate areas of low resistivity and the blue colours represent resistive material. Model (a) shows results of inversion using TM and TE-mode data at 105° with high error floors set on the apparent resistivities, (b) shows results using TM and TE-mode data at 105° with lower error floors on the apparent resistivities, (c) shows results using TM, TE, and HZ-data at 105°, (d) shows results of inverting the northern most sites using the TM and TE-mode data at 45°, and (e) shows results of inverting the southern most sites using the TM and TE-mode data at 105°.

Appendix I

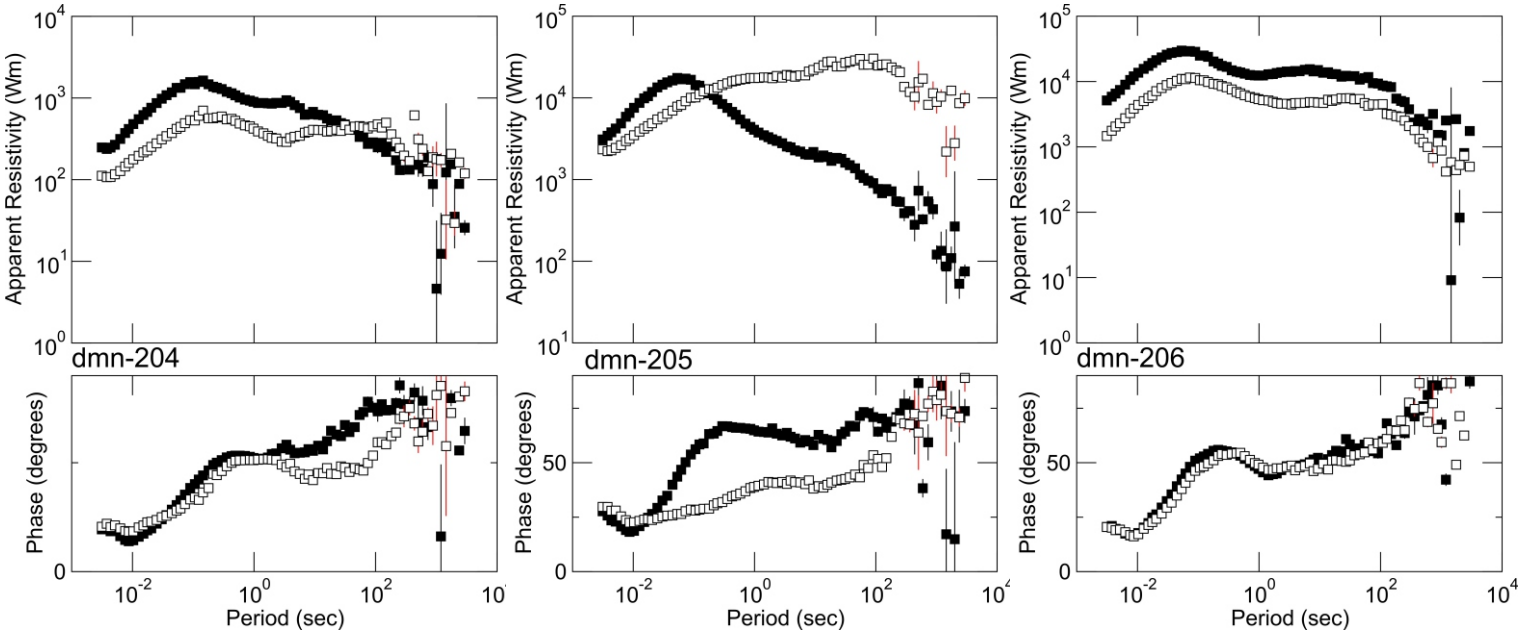
Apparent Resistivity (Wm)
Phase (degrees)
Period (sec)
dmn-204
dmn-205
dmn-206

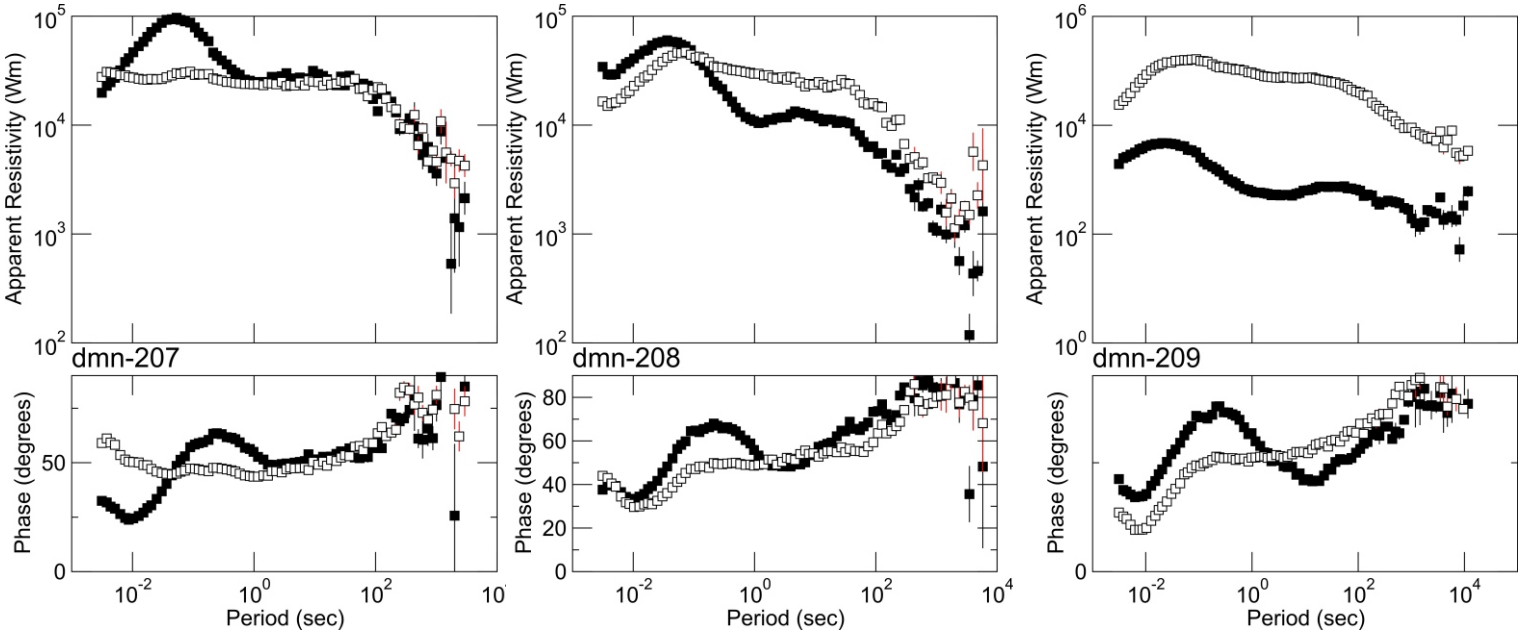
Apparent Resistivity (Wm)
Phase (degrees)
Period (sec)
dmn-207
dmn-208
dmn-209

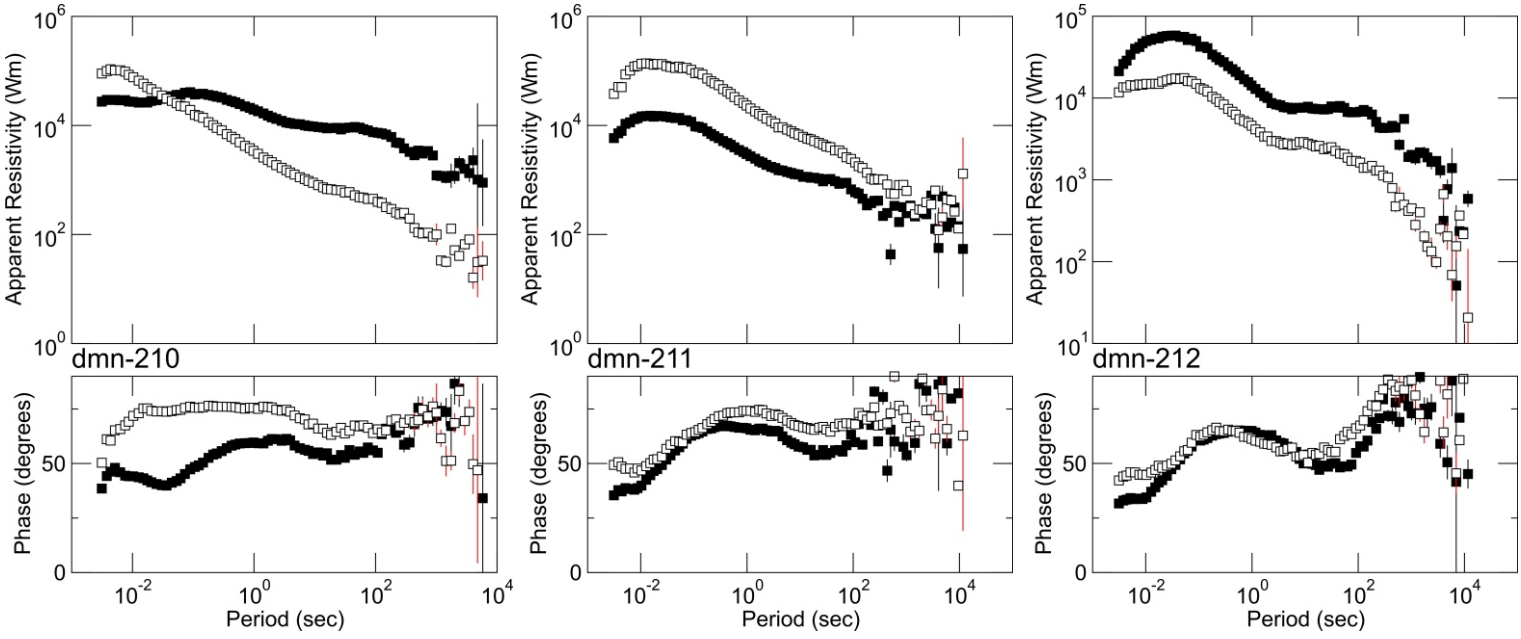
Apparent Resistivity (Wm)
Phase (degrees)
Period (sec)
dmn-210
dmn-211
dmn-212

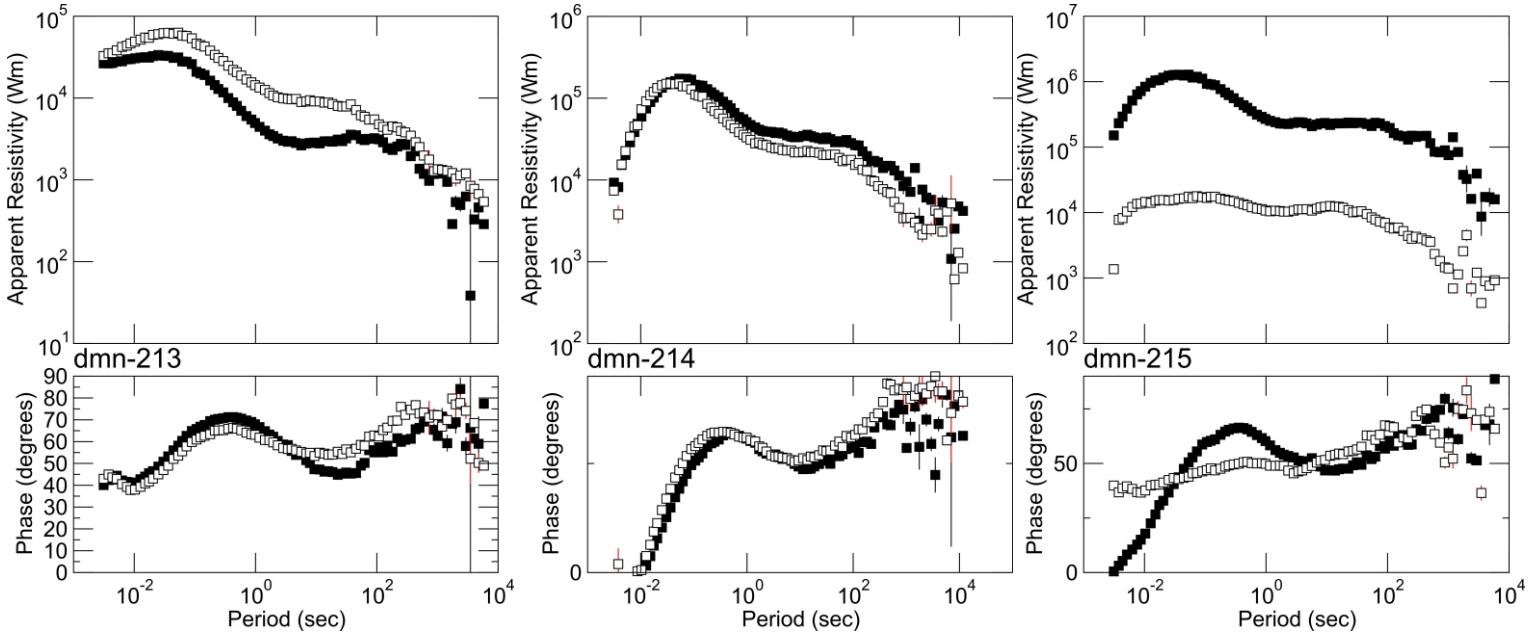
Apparent Resistivity (Wm)
Phase (degrees)
Period (sec)
dmn-213
dmn-214
dmn-215

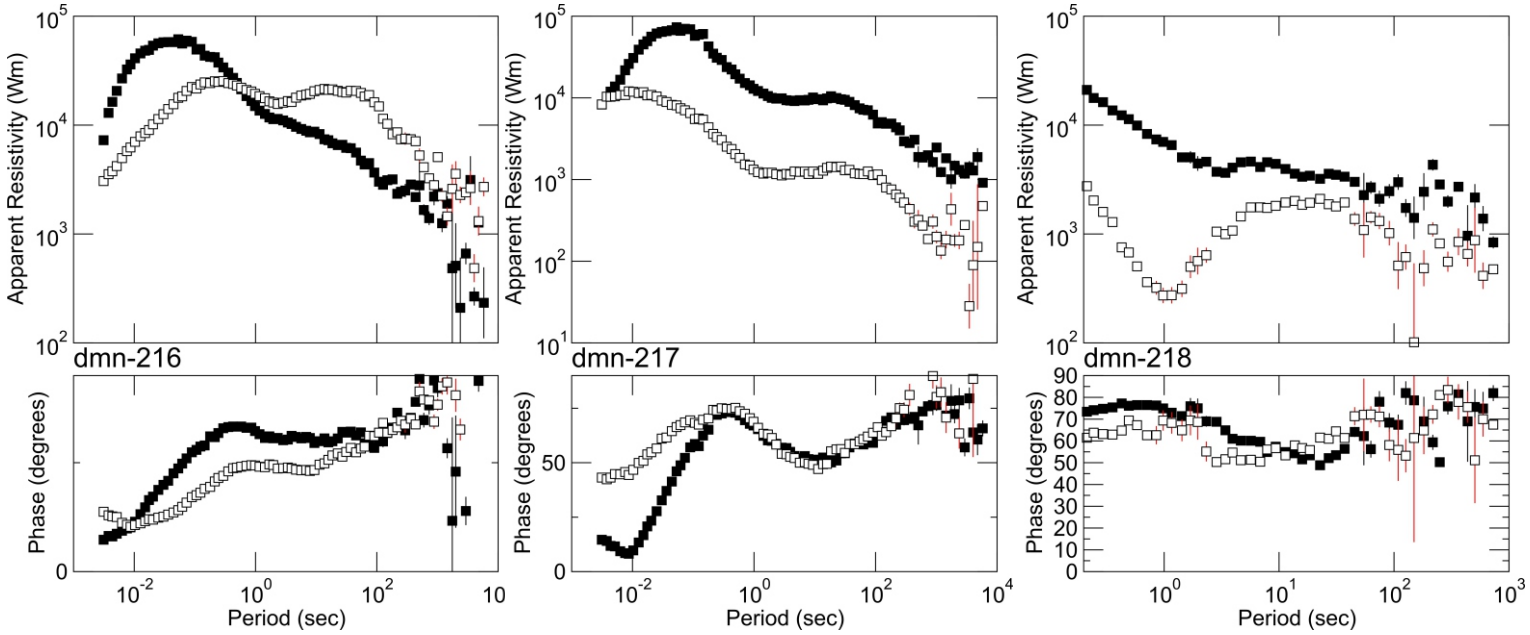
Apparent Resistivity (Wm)
Phase (degrees)
Period (sec)
dmn-216
dmn-217
dmn-218

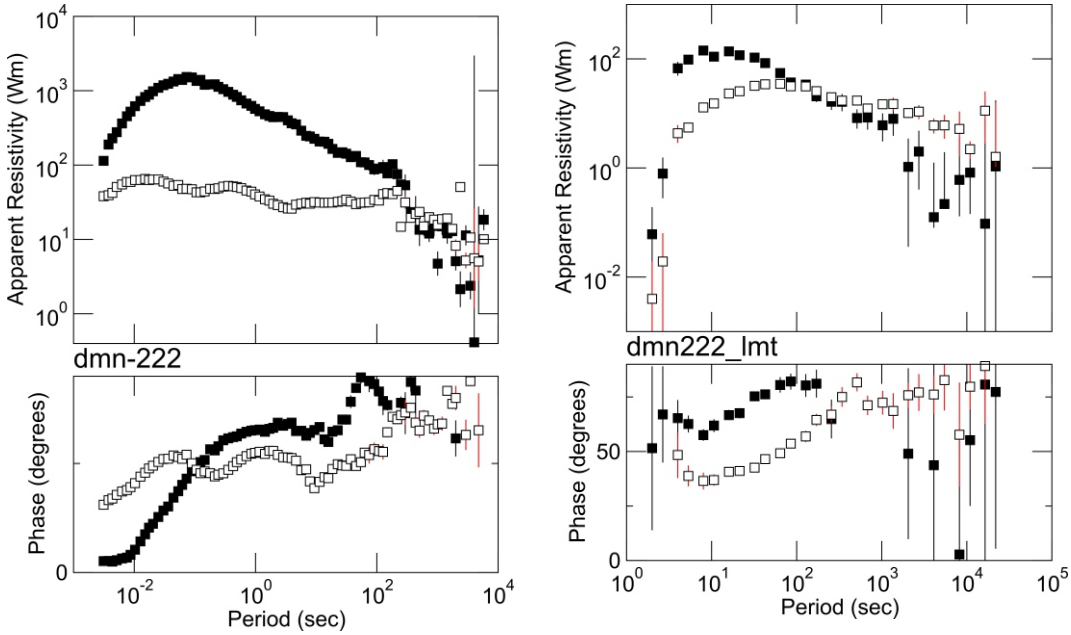
Apparent Resistivity (Wm)
Phase (degrees)
Period (sec)
dmn-222
dmn222_lmt